Miniaturized engineered heart tissues from hiPSC-derived triple cell type co-cultures to study human cardiac function

Windt, L. M.; Wiendels, M.; Dostanić, M.; Bellin, M.; Sarro, P. M.; Mastrangeli, M.; Mummery, C. L.; van Meer, B. J.

DOI
10.1016/j.bbrc.2023.09.034

Publication date
2023

Document Version
Final published version

Published in
Biochemical and Biophysical Research Communications

Biochemical and Biophysical Research Communications 681 (2023) 200–211

Contents lists available at ScienceDirect

Biochemical and Biophysical Research Communications

journal homepage: www.elsevier.com/locate/ybbrc

Miniaturized engineered heart tissues from hiPSC-derived triple cell type co-cultures to study human cardiac function

L.M. Windt [a,1], M. Wiendels [a,1], M. Dostanić [a,b], M. Bellin [a,c,d], P.M. Sarro [b], M. Mastrangeli [b], C.L. Mummery [a], B.J. van Meer [a,e,*]

[a] Department of Anatomy and Embryology, LUMC, Leiden, the Netherlands
[b] Microelectronics, TU Delft, Delft, the Netherlands
[c] Department of Biology, University of Padua, Padua, Italy
[d] Veneto Institute of Molecular Medicine, Padua, Italy
[e] Sync Biosystems, Leiden, the Netherlands

ARTICLE INFO

Keywords:
Engineered heart tissues
hiPSCs
Cardiomyocytes
Microphysiological system
Cardiac contraction

ABSTRACT

Human heart tissues grown as three-dimensional spheroids and consisting of different cardiac cell types derived from pluripotent stem cells (hiPSCs) recapitulate aspects of human physiology better than standard two-dimensional models *in vitro*. They typically consist of less than 5000 cells and are used to measure contraction kinetics although not contraction force. By contrast, engineered heart tissues (EHTs) formed around two flexible pillars, can measure contraction force but conventional EHTs often require between 0.5 and 2 million cells. This makes large-scale screening of many EHTs costly. Our goals here were (i) to create a physiologically relevant model that required fewer cells than standard EHTs making them less expensive, and (ii) to ensure that this miniaturized model retained correct functionality. We demonstrated that fully functional EHTs could be generated from physiologically relevant combinations of hiPSC-derived cardiomyocytes (70%), cardiac fibroblasts (15%) and cardiac endothelial cells (15%), using as few as 1.6×10^4 cells. Our results showed that these EHTs were viable and functional up to 14 days after formation. The EHTs could be electrically paced in the frequency range between 0.6 and 3 Hz, with the optimum between 0.6 and 2 Hz. This was consistent across three downscaled EHT sizes tested. These findings suggest that miniaturized EHTs could represent a cost-effective microphysiological system for disease modelling and examining drug responses particularly in secondary screens for drug discovery.

1. Introduction

Cardiovascular diseases, including heart failure, are the leading cause of death worldwide according to the World Health Organization (WHO). Many of these diseases, such as myocardial infarction and coronary heart disease, affect multiple cell types in the heart [1]. In studying the pathogenesis of cardiac disease, it may be important to consider crosstalk between these cell types as part of the underlying disease mechanism. Genetic mouse models have typically been used to investigate diseases affecting single or multiple cell types by introducing mutations in specific cardiac lineages. Primary heart cells can also be used to study cardiac diseases. However, these cells are difficult to access and have limited availability and lifespan. To develop renewable and easy access models to study the pathogenesis of cardiac disease, human induced pluripotent stem cells (hiPSCs) are becoming a favoured option. hiPSCs can not only differentiate toward different cardiac cell types but can also be derived from patients with specific genetic diseases [2].

We and others have shown previously that it is possible to derive cardiomyocytes (CMs), cardiac endothelial cells (ECs), and cardiac fibroblasts (CFs) efficiently from hiPSC and that these can be combined to form three-dimensional (3D) cardiac tissues *in vitro* [3–5]. In 3D spheroids containing these three cell types, the hiPSC-CMs mature and contraction kinetics can be measured but the effects of mechanical load or contraction force cannot be measured. Engineered Heart Tissues (EHTs) offer an alternative in which force can be measured [6]. EHTs are

* Corresponding author. Department of Anatomy and Embryology, LUMC, Leiden, the Netherlands.
E-mail address: B.j.van_meer@lumc.nl (B.J. van Meer).
[1] These authors contributed equally to this work and share first authorship.

https://doi.org/10.1016/j.bbrc.2023.09.034
Received 1 July 2023; Received in revised form 23 August 2023; Accepted 14 September 2023
Available online 20 September 2023

formed by allowing suspensions of cardiac cells in extracellular matrix solutions to self-organize around elastomeric pillars. The pillars act as anchoring points for 3D tissue formation and thus recapitulate the mechanical load [3]. Tracking pillar deflection upon tissue contraction makes this model particularly suitable for measuring changes in beat rate, contraction force, passive tension and maximum capture rate [4,6,7]. In addition, EHTs have been described as showing improved reliability in drug testing and suitability for long-term drug exposure as they are more stable than scaffold-free tissues [8,9]. Multiple strategies have been described to generate EHTs of different sizes using different numbers of cells as input [10–12]. In general, though, they often include large numbers of cells, typically 0.5–2 $\times$ 10^6 per EHT [4,5,13]. There would be significant cost benefits in reducing these numbers and the corresponding cell culture volume. One of the few studies describing scale reduction was by Chen and colleagues, who were able to generate EHTs from only ~500 cells [14,15]. However, these studies used neonatal rat cardiomyocytes (CMs). These are less difficult to culture and more mature than hiPSC-CMs, but they do not allow modelling human genetic diseases or capture human genetic backgrounds which may affect the phenotype. In addition, the experiments were terminated on day 7, so that any decrease in cell viability over longer periods would not have been detected. We postulated that there would be value in developing entirely hiPSC-based EHTs in these miniaturized formats and monitoring their functionality and viability over longer time spans.

Here, we describe this process. We used our previous EHT platform based on the Heart-Dyno system where cardiac cells self-assemble around flexible pillars as a starting point to miniaturize EHTs [7,16]. We investigated the effect of anisometric downscaling on the functionality of EHTs made of hiPSC-CMs (70%), hiPSC-cardiac ECs (15%) and hiPSC-CFs (15%), a combination we have shown previously to promote hiPSC-CM maturation in 3D spheroids. We were able to generate viable and functional miniaturized EHTs with total cell numbers of approximately 4.7 $\times$ 10^4, 3.1 x 10 ^{4} and 1.6 $\times$ 10^4 in 3-, 2-, and 1 μL volumes. Focus features were integrated on top of the micropillars to enable accurate measurement of contractile parameters reflected in pillar displacement. Comparisons of three downscaled EHT sizes demonstrated that downscaling is possible, reducing cell input requirements without loss of functionality.

2. Materials and methods

2.1. hiPSC culture and differentiation

hiPSCs were seeded on recombinant human vitronectin-coated plates and cultured in E8 medium [17]. The cells were dissociated using 1$\times$ TrypLE Select and passaged twice weekly using Revitacell (1:200) (all Thermo Fisher Scientific).

Differentiation to hiPSC-CMs was as described previously [2,18]. Briefly, 4 $\times$ 10^4 hiPSCs per cm^2 were seeded on growth factor-reduced Matrigel- (75 mg/ml, Corning) coated plates in E8 medium supplemented with Revitacell (1:200), on day −1. Cardiac mesoderm was induced on day 0 by changing from E8 medium to BPEL supplemented with 20 ng/ml BMP4 (R&D Systems), 20 ng/ml human Activin A (Miltenyi Biotec) and 1.5 mM GSK3 inhibitor CHIR99021 (Axon Medchem). On day 3, medium was replaced by BPEL supplemented with 5 μM Wnt inhibitor XAV939 (Tocris). On day 6, medium was replaced by BPEL only. Medium was refreshed every 2–3 days. On day 17, hiPSC-CMs were dissociated with a mixture of enzyme T (10%) with buffer X (90%; both Miltenyi), the percentage of Troponin T positive cells was determined by FACS with cTNT antibody (clone REA400-VioBlue; 1:50; Miltenyi Biotec) and cells were cryopreserved ~3 $\times$ 10^6 cells per vial in KnockOut™ Serum Replacement (KO-SR) (Thermo Fisher Scientific) with 10% DMSO (0.3 ml/vial; Sigma-Aldrich).

hiPSC-cardiac EC differentiation was also done as described previously [2,19]. Briefly, 1.2 $\times$ 10^4 hiPSCs per cm^2 were seeded on growth factor-reduced Matrigel-(75 mg/ml) coated plates in E8 medium supplemented with Revitacell (1:200), on day −1. On day 0, cardiac mesoderm was induced by replacing E8 medium with BPEL supplemented with 20 ng/ml BMP4, 20 ng/ml human Activin A and 1.5 mM GSK3 inhibitor CHIR99021. On day 3, medium was replaced by BPEL supplemented with 50 ng/mL VEGF (R&D Systems) and 5 μM Wnt inhibitor XAV939. On day 6, isolation of CD34 positive cells was performed using the human cord blood-CD34-positive selection kit II (StemCell Technologies) following manufacturer's instructions. Isolated cells were seeded 20 $\times$ 10^3 cells per cm^2 on fibronectin (1:200; Sigma-Aldrich) coated plates and cultured in BPEL supplemented with 50 ng/mL VEGF. Medium was refreshed every 2–3 days. On day 9, cells were dissociated with 1$\times$ TrypLE Select, the percentage of CD31 positive cells was determined by FACS with PECAM-1 antibody (clone WM59-APC; 1:100; eBioscience) and cells were cryopreserved (20 cm^2 per vial) in CryoStor CS10 medium (0.5 ml/vial; Stem Cell Technologies).

hiPSCs-CF differentiation was done as described previously [2]. Briefly, 2 $\times$ 10^4 hiPSCs per cm^2 were seeded on growth factor-reduced Matrigel-(75 mg/ml) coated plates in E8 medium supplemented with Revitacell (1:200), on day −1. On day 0, cardiac mesoderm was induced by replacing E8 medium with BPEL supplemented with 20 ng/ml BMP4, 20 ng/ml human Activin A (Miltenyi Biotec) and 1.5 mM GSK3 inhibitor CHIR99021. On day 3, medium was replaced by BPEL supplemented with 30 ng/ml BMP4, 1 μM Retinoic acid (Sigma-Aldrich) and 5 μM Wnt inhibitor XAV939. On day 6, medium was replaced by BPEL supplemented with 30 ng/ml BMP4 and 1 μM Retinoic acid. On day 9, cells were dissociated using 1$\times$ TrypLE Select and 15 $\times$ 10^3 cells per cm^2 were seeded on plates coated with fibronectin (1:200) in BPEL medium supplemented with 10 μM of TGF-β inhibitor SB431642 (Tocris). On day 12, hiPSC-epicardial cells (hiPSC-EPIs) were confluent and cryopreserved (20 cm^2 per vial) in CryoStor CS10 medium (0.5 ml/vial) or 20 $\times$ 10^3 hiPSC-EPIs per cm^2 were seeded on vitronectin-coated plates (0.5 μg/cm^2) in BPEL supplemented with 10 ng/ml FGF2 (R&D Systems). On day 13 and every 2–3 days, medium was refreshed with BPEL supplemented with 10 ng/ml FGF2. On day 19, medium was changed to Fibroblast Growth Medium 3 (FGM3; PromoCell). FGM3 medium was refreshed every 2–3 days. hiPSC-CFs were passaged when confluent and cryopreserved after three passages (10–30 cm^2 per vial) in CryoStor CS10 medium (0.5 ml/vial).

2.2. EHT platform

The EHT platforms were fabricated as described previously [16]. Briefly, using a design inspired by the Heart-Dyno system, we an isometrically downscaled the EHTs to fit 3, 2 and 1 μL volumes within elliptical microwells [7]. EHT platforms were made by moulding polydimethylsiloxane (PDMS) into the etched cavities in silicon wafer. Rectangular focus features were patterned at the bottom of the silicon mould and transferred to the top of the PDMS micropillars after moulding (Fig. S3A). The micropillars were characterized utilizing the FemtoTools nanoindentation system (FT-NMT03). An EHT platform was placed on the bottom of each single well of a 96-well plate and sterilized with 70% ethanol for 10 min, washed three times with PBS without calcium and magnesium (Thermo Fisher Scientific) for 5 min, and air dried while exposed to UV light for 20 min.

2.3. EHT formation

On day −7, hiPSC-CFs were thawed (~2 $\times$ 10^5 per 10 cm^2) and cultured in FGM3 medium. On day −4, hiPSC-CMs were thawed on growth factor-reduced Matrigel (75 mg/ml, Corning) coated plates (~3 $\times$ 10^6 per 4 cm^2) and cultured in BPEL. On day −2, hiPSC-ECs were thawed (~4 $\times$ 10^5 per 10 cm^2) on fibronectin-(1:200) coated plates and cultured in BPEL supplemented with 50 ng/mL VEGF. The cells were ready to use on day 0, when the cells had recovered from thaw, hiPSC-CMs had started spontaneous contraction and hiPSC-CFs were reaching

confluence (Figs. S1A–D) [2]. The cells were dissociated as described earlier and combined in a controlled ratio of 70% hiPSC-CMs, 15% hiPSC-ECs and 15% hiPSC-CFs and centrifuged at 450*g*. The cells were mixed with formation medium (39%) and with pre-mixed acid solubilized collagen I (41%, 3.3 mg/mL), 6% NaOH, 5% DMEM (10×), 9% Matrigel (10 mg/mL) following the protocol by Mills et al. [7]. The final cell-ECM mix consists of approximately 1.57×10^4 cells/μL and was added in the correct volume to the corresponding EHT well: 3, 2 or 1 μL. Formation medium supplemented with 50 ng/μL VEGF and 5 ng/μL FGF2 was added for the first 72 h [7]. On day 3, the medium was changed to BPEL supplemented with 50 ng/μL VEGF and 5 ng/μL FGF2. Medium was refreshed every 48 h and 1 h before performing assays.

2.4. Immunofluorescence analysis

For whole mount immunofluorescence staining, EHTs were taken out of the wells and transferred to a V-bottom 96-well plate. After a PBS wash, the EHTs were fixed for 1 h in 4% paraformaldehyde on a shaker, washed 3 times for 10 min with PBS+ (Thermo Fisher Scientific) containing 4% FCS and stored at 4 °C until processing. Permeabilization was done with PBS + containing 0.3% Triton X-100 (Sigma-Aldrich), for 30 min on a shaker. Next, blocking was done for 3 h with PBS + containing 10% FCS, 2% BSA and 0.1% Tween. Primary antibodies Cardiac Troponin T (1:1500; Abcam) and human CD31 (1:200; R&D Systems) were added and incubated overnight at 4 °C on a shaker. EHTs were washed 3 times with PBS + containing 4% FCS for 20 min on a shaker. Secondary antibodies were added and incubated overnight in the dark, at 4 °C and on a shaker. EHTs were washed 3 times for 20 min with PBS + containing 4% FCS in the dark and on a shaker. Next, they were stained with DAPI (1:500) for 10 min at room temperature in the dark on a shaker, then transferred to a glass coverslip and placed in the middle of a 250 μm thick iSpacer® double-sided sticker (Sunjinlab). Excess liquid was removed with a tip of tissue paper prior to incubating the EHTs in a drop of CytoVista™ Tissue Clearing Reagent (Thermo Fisher Scientific) for 10 min in the dark. Next, the Clearing agent was removed and EHTs were mounted in the middle of the sticker between two coverslips in Prolong glass antifade mountant (Invitrogen) according to manufacturer's protocol. Images were acquired using a Leica SP8 microscope connected to an Andor Dragon-fly 500 spinning disc confocal system (Andor Technology) using immersion oil, a 20×/oil magnification objective and Z stack acquisition.

2.5. Cell viability analysis

Nuclear live/dead staining (Thermo Fisher Scientific) was done by adding 4 drops of dye per mL medium. Additionally, 20 μM para-nitroblebbistatin (Ceyman chemical) was added to stop contraction. After 1 h incubation, images were acquired with a Leica SP8 microscope connected to an Andor Dragon-fly 500 spinning disc confocal system (Andor Technology) using a 10× magnification objective and Z stack acquisition. Quantification was performed using the Spots tool of Imaris Microscopy Image Analysis Software (Oxford Instruments). Overview scans and videos of stained contractile EHTs were acquired using an EVOS M7000 microscope (Thermo Fisher Scientific) with a 4× magnification.

2.6. Contraction analysis

Recordings of 100 frames per second were taken with a Nikon Eclipse Ti optical microscope connected to a Thorlabs USB 3.0 digital camera, while focusing on the top of the micropillars. EHTs were kept in a custom-built environmental chamber at 37 °C and 5% CO_2 during recording of the videos. For each timepoint, a video of 10 s was recorded. Electrical pacing was performed with custom-made platinum electrodes. Sequential biphasic rectangular pulses with 10 ms pulse duration and ±20 V peak amplitude were applied to the EHTs. 30 s adjustment time was applied between different frequencies before recording. Medium was refreshed 1 h in advance of taking recordings. Movement of the pillars was tracked and analysed by pixel intensity change with MUSCLEMOTION software [6]. Contraction force was calculated based on the pillar displacement and effective stiffness of the pillars at the point of force application. The stiffness of micropillars measured using the FemtoTools nanoindentation system (FT-NMT03) was found to be ~10 N/m in the middle of the pillar height [16]. Pillar displacement was quantified using custom-made software: ForceTracker.

2.7. Statistics

Detailed statistics and statistical significance are indicated in each figure legend. Data are expressed and plotted as the Mean ± SEM. Significance was attributed to comparisons with values of $P < 0.05$*; $P < 0.01$**; $P < 0.001$***. Statistical analysis was performed using RStudio online version 2023.03.0 + 386 (R version 4.2.3).

3. Results

3.1. hiPSC-derived CMs, ECs and CFs form miniaturized EHTs

To assess whether downscaling of EHT size affected functionality, we seeded hiPSC-CMs, -ECs, and -CFs together in an extracellular matrix (ECM) mix of collagen I and Matrigel in microwell volumes of 1, 2 and 3 μL (Fig. 1A, B, C and S1A, B, C, D). The EHT formation timeline is shown schematically in Fig. 1D. Within the first few hours, the cell-ECM mixture compacted around the two flexible PDMS micropillars, providing structural support for 3D tissue formation (Fig. 2A). Spontaneous, synchronous contraction of the tissues in the longitudinal direction started within 72 h (Fig. S1E). Tissue dimensions (length x width x thickness) were measured and corresponded to the associated EHT platform size. Average dimensions for EHT size 1 (1 μL) were 1130 x 485 × 139 μm, size 2 (2 μL) 1410 x 629 × 185 μm, and size 3 (3 μL) 1548 x 657 × 192 μm (Fig. 2B). The distribution of cells throughout the EHT was monitored by immunofluorescent staining for cell type specific markers (cardiac troponin T, CTNT, for hiPSC-CMs; cluster of differentiation 31, CD31, for hiPSC-ECs and vimentin for hiPSC-CFs) (Fig. 2C and S1F). The results demonstrated successful tissue formation with 1.6×10^4, 3.1×10^4 and 4.7×10^4 cells per EHT i.e. sizes 1, 2 and 3, respectively.

3.2. Miniaturized EHTs are viable and functional

Cell viability was then assessed in EHTs (Fig. 3A, S2A, B). The percentage of live cells in size 1 and 2 EHTs significantly increased from day 4 to day 14 (Fig. 3B). In size 3 EHTs, the percentage of live cells was unchanged when comparing day 4 and day 14. In addition, the total number of live cells increased relative to baseline in all three EHT sizes, while the number of dead cells did not change (Figs. S2C and D). Dead cells were distributed throughout the EHTs but no necrotic clusters were evident anywhere in the EHT.

Regardless of the size, EHTs showed spontaneous rhythmic contraction. Representative qualitative analysis of spontaneous contraction is shown in Fig. 3C. In general, contraction was observed between day 4 and 14, but sporadically EHTs were quiescent, which was more frequent at later timepoints (Fig. 3D and S3A, B). The mean spontaneous contraction rate of the three EHT sizes decreased from 0.4 Hz to 0.1 Hz between day 4 and 14 (Fig. 3D and S3C). On all days, except day 12, there were no differences in spontaneous contraction rate between the three EHT sizes (Fig. S3D). No differences were detected in the spontaneous contraction amplitude of EHTs size 1 between day 4 and 14 (Fig. 3E I). The contraction amplitude of EHTs size 2 reached its maximum on day 6, but significantly decreased after day 10 (Fig. 2E II). Similarly, the contraction amplitude of EHTs size 3 increased from day 4

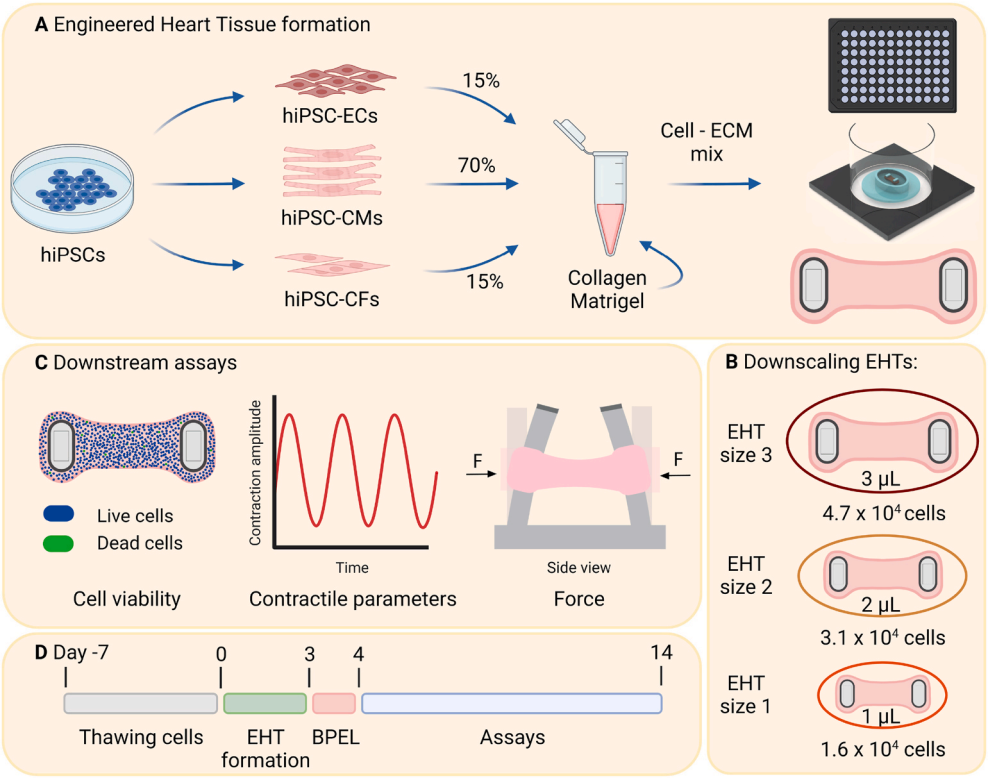

Fig. 1. Formation of miniaturized Engineered Heart Tissues (EHTs) using hiPSC-derived CMs, ECs, and CFs.
(A) EHT formation consisting of hiPSC-derived ECs, CMs and CFs mixed with ECM before addition on the EHT platform. **(B)** EHTs are downscaled on platforms with volumes of 3, 2 and 1 µL and contain 4.7×10^4, 3.1×10^4 and 1.6×10^4 cells, respectively. **(C)** Downstream assays to asses viability and functionality of the EHTs. **(D)** Timeline thawing of cells, EHT formation and assays.

to day 8, with the maximum between day 6 and day 8 before decreasing (Fig. 3E III). The contraction duration of EHTs size 1 (Fig. 3F I) and size 2 (Fig. 3F II) increased from day 4 to day 10. The contraction duration in size 3 EHTs increased from day 4 to day 14 (Fig. 3F III).

3.3. Miniaturized EHTs respond to electrical pacing

The tissues were subjected to electric field stimulation every 48 h during the experiment, starting from day 4 until day 14 after formation. EHTs of all sizes could be electrically stimulated (Figs. S4A, B, C). To make sure we could evaluate the responses of all EHTs, we used a broad pacing range between 0.6 and 3 Hz. Frequencies below 0.6 Hz gave no contraction response since spontaneous beating was at or above this rate. The results were therefore not included. The pacing frequency was increased from 0.6 to 3 Hz in steps of 0.2 Hz. Subsequently, the contraction amplitude (a.u.) for all three sizes was measured at a series of pacing frequencies. Although all EHT sizes could be electrically stimulated, certain frequencies were not captured when pacing rates were much lower or higher than spontaneous contraction rate of the EHTs (Figs. S4A, B, C). The overall capture rate was >85% when EHTs were electrically paced between frequencies of 0.6 and 2 Hz (Fig. 4A).

Next, the contraction amplitude of the three EHT sizes was compared every 48 h from day 4 to day 14 under electrical pacing between 0.6 and 3 Hz. On day 8, significant differences in contraction amplitude between EHT sizes were detected when paced between 0.6 and 2 Hz (Fig. 4B). The differences in contraction amplitude between the EHT sizes were most striking on day 8. Overall, contraction amplitude was most disparate between the smallest (EHTs size 1) and largest (EHTs size 3) tissues, with the lowest and highest contraction amplitudes, respectively. No significant differences in contraction amplitudes between the EHTs sizes was found on day 14.

3.4. Contraction kinetics of EHTs paced at 1Hz are similar to spontaneous contracting EHTs

Representative qualitative analysis of EHTs electrically paced at 1 Hz is shown in Fig. 5A. Much like the spontaneous contraction amplitudes (Fig. 3E), no significant differences in contraction amplitude over time were detected in size 1 EHTs electrically paced at 1 Hz (Fig. 5B I). A decrease in contraction amplitude was found in size 2 EHTs from day 6 to day 14 (Fig. 5B II). Lastly, contraction amplitude increased from day 4 to day 6 and decreased from day 6 to day 14 in size 3 EHTs (Fig. 5B III). These findings suggest that electrical pacing at physiologically relevant frequencies, such as 1 Hz, shows similar fluctuations in contraction amplitude over time as seen in spontaneously contracting EHTs with a lower contraction rate. It should be noted that, subjected to 1 Hz pacing, the highest contraction amplitude in size 2 EHTs was reached on day 6, and for size 3 EHTs, it was between day 6 and 8 (Fig. 5B). This was again similar to that in spontaneously contracting EHTs and also with electrical pacing at other physiological frequencies (Fig. 3F and S5A). Furthermore, contraction duration was stable over time for all three EHTs sizes with 1 Hz pacing (Fig. 5C) and other physiologically relevant pacing frequencies (Fig. S5B). Representative qualitative analysis of EHTs that were paced at 0.8, 1.2 and 1.4 Hz support these findings (Fig. S5C).

3.5. Force is relative to EHT size on day 6 and 8, while normalized force per cardiomyocyte is constant

In addition to the contraction amplitude, the forces generated by EHTs of the three different sizes were measured based on pillar displacement. Contractile forces of spontaneously contracting EHTs were similar for all three sizes on days 4, 10 and 14 although for size 3 the mean force was never below that of size 1. On days 6, 8 and 12, this

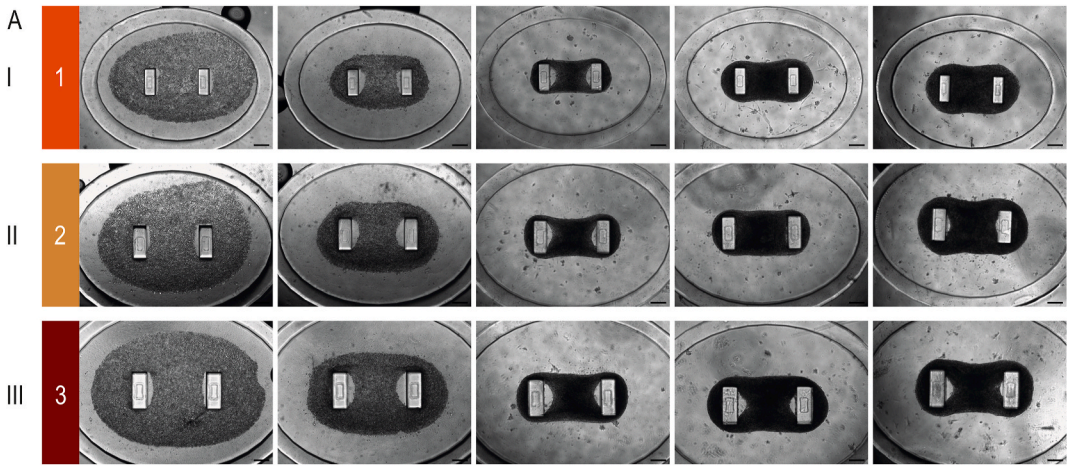

B

EHT size	Length (µm)	Width (µm)	Height (µm)
1	1130	485	139
2	1410	629	185
3	1548	657	192

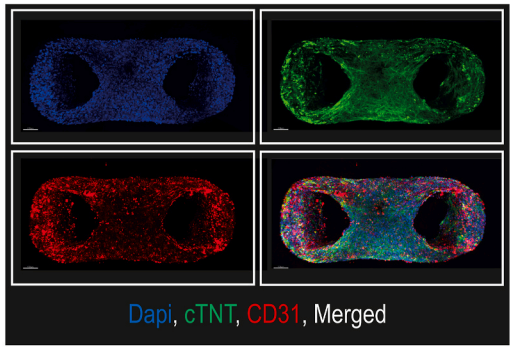

Fig. 2. EHTs downscaling can be achieved by decresing cell number and culture volume.
(A) Phase contrast images of EHTs size I) 1, II) 2 and III) 3 self-assembly: 1 and 2 h, 3, 6 and 14 days after seeding the cell-ECM mixture on the 1, 2 and 3 µL EHT platforms. Scale bar: 200 µm. **(B)** Dimensions of the three EHT sizes in micrometer (µm). **(C)** Representative immunofluorescent images of EHTs stained for Cardiac Troponin T (cTNT) (green), CD31 (red), nuclei with Dapi (blue) and a merged image. Scale bar: 100 µm. (For interpretation of the references to colour in this figure legend, the reader is referred to the Web version of this article.)

was statistically significant with lower forces for smaller EHTs and higher forces for the larger EHTs, respectively (Fig. 6A). The contractile force did not change over time for size 1 EHTs but did decrease after day 6 for size 2 and 3 EHTs (Fig. S6).

Contractile forces of EHTs subjected to electrical pacing were then analysed. Specifically, we investigated whether there were differences in forces between the different EHT sizes when they were contracting at the same frequency. As with the spontaneously contracting EHTs, the mean force of the large EHTs was always above that of the smaller EHTs and in some cases this difference was significant, but we sometimes noted large fluctuations in values within one EHT size or between sizes. This was particularly evident on day 8 (Fig. 6B) at all pacing stimulations between 0.6 and 2.4 Hz and on day 6, with significant differences in contraction force between sizes 1 and 3 in a pacing range of 0.6 and 2.8 Hz. In addition, the highest active force of ~300 µN was reached on day 6 and 8 in size 3 EHTs. On days 4 (early) and 14 (late), contractile forces in general did not differ between EHT sizes at pacing rates between 0.6 and 3 Hz. The contractile force of size 1 EHTs was below the detection limit on day 14.

Fluctuations in force observed within one EHT, evidenced as larger statistical spread in some data points, might be due to the differences in z-direction position of the tissues on the pillars which we are presently unable to control.

The effective stiffness of the micropillars remained constant in all three miniaturized EHT platforms, due to anisometric scaling of the platform as described earlier i.e. the diameter of the wells was decreased and the width/thickness of the pillars proportionally reduced [16]. The contractile force normalized for the number of cardiomyocytes per EHT is shown in Fig. 6C. Interestingly, we found that on day 6, 8 and 14, there were no differences in contractile force between the EHT sizes when normalized for the number of cardiomyocytes per EHT (Fig. 6C) and on day 10 and 12, differences were only sporadic, and again possibly due to z-direction position. We did note that cells in size 1 EHTs delivered significantly more energy in the form of contractile force on day 4, when paced between 0.6 and 1 Hz, at 1.8 Hz and 2.4 Hz, compared to size 2 and 3 EHTs (Fig. 6C). In addition, on day 10 and 12, there was incidentally a significant increase in contractile force per cell in size 1 EHTs when paced at higher frequencies. On day 14, the normalized contractile force of size 1 EHTs was below the detection limit.

4. Discussion

3D cardiac tissues *in vitro* exhibit many features of native human myocardium, albeit at early postnatal- or juvenile stages of development. We have previously addressed this issue in depth by creating cardiac microtissues from hiPSC that contain hiPSC-CMs (70%), hiPSC-CFs (15%) and hiPSC-ECs (15%) [2]. All three cell types contributed to maturation in different ways: firstly, hiPSC-ECs produce Endothelin-1, which binds to its receptor on hiPSC-CMs and via the adenylate cyclase pathway, increases intracellular cAMP; secondly, NO is produced by hiPSC-ECs, which activates cGMP in cardiac fibroblasts. Since cardiac fibroblasts form gap junctions with hiPSC-CMs, cGMP can transfer into the hiPSC-CMs and also contribute to increasing intracellular cAMP. Thus, the three cell types contribute in different ways to inducing features of hiPSC-CM maturation in these 3D microtissues, such as higher action potentials, lower resting membrane potentials,

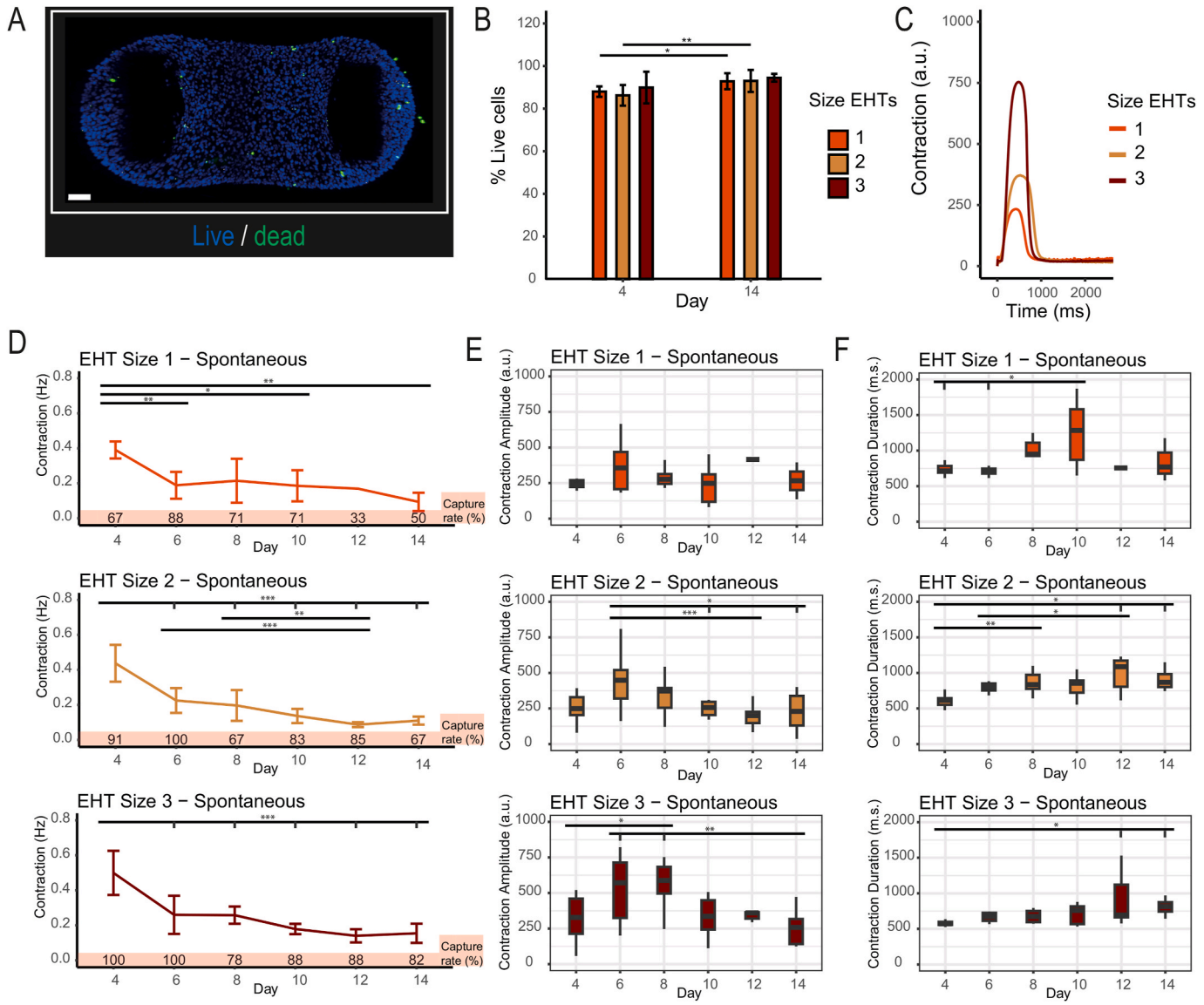

Fig. 3. Improved cell viability and spontaneous contraction in EHTs between day 4 and day 14.
(A) Representative image of nuclear stained cells: live (blue) and dead (green) during live imaging. **(B)** Percentage live cells on day 4 and day 14 in EHTs size 1, 2 and 3. EHT size 2: N > 3; EHTs size 1 and 3: N = 2–3; *p < 0.05; **p < 0.01; ***p < 0.001. Data is shown as mean ± SEM. N indicates EHTs from 2 to 4 independent batches per group and 6–12 technical repeats. Unpaired *t*-test is shown. **(C)** Representative qualitative analysis of spontaneous contraction of EHTs size 1, 2, and 3 on day 6. **(D)** Spontaneous contraction frequency (Hz) of EHTs size 1, 2 and 3 between day 4 and 14. Percentage of spontaneous contracting EHTs is shown above the x-axis. **(E)** Spontaneous contraction amplitude of EHTs size 1, 2 and 3 between day 4 and 14. **(F)** Spontaneous contraction duration of EHTs size 1, 2 and 3 between day 4 and 14. Data of C–F: N = 4; *p < 0.05; **p < 0.01; ***p < 0.001. Data is shown as mean ± SEM. N indicates EHTs from 4 independent batches per group. One-way Anova with Tukey *post hoc* test is shown. (For interpretation of the references to colour in this figure legend, the reader is referred to the Web version of this article.)

greater sarcomere organization and the presence of t-tubules, essential for proper calcium handling postnatally. EHTs have also been reported to show improved maturation and, probably as a result, greater reliability in drug testing [8,9]. This prompted us previously to generate EHTs consisting of hiPSC-CMs (80%) and hiPSC-CFs (20%) but without hiPSC-ECs [16]. In the study presented here, we used 70% CMs, 15% CFs and included 15% ECs to recapitulate microtissue conditions [20,21].

The overall goal was to develop a miniaturized EHTs platform that still can function as a useful model. Three different sizes of EHTs were tested, where size 1 is the smallest feasible EHTs size to pipette. The cell numbers were reduced *pro rata* between the different sizes. One idea behind downscaling is that nutrient and oxygen penetration to all cells in the EHT may improve, avoiding effects on contractility and force. Nutrients and oxygen penetrate the compact muscle strands in the EHTs by diffusion only by 100–200 μm [22,23]. To retain full cell viability in larger EHT, diffusion distance is rate limiting. Larger EHTs would therefore ideally have vasculature incorporated. Several strategies have already been described for this: (i) adding vascular cells to the cardiac tissue allowing perfusion via endothelialized channels and (ii) an artificial vessel was constructed between the pillars allowing perfusion of the EHTs for up to 3 weeks [24–26].

Instead of using vascular cells or perfusion, miniaturizing EHTs was sufficient to retain cell viability. The EHTs generated were between 192 μm and 139 μm in thickness. Size 3 was thus close to the maximum diffusion thickness of 200 μm; however, all 3 sizes are between 100 and 200 μm indicating that all are within the maximum limit for diffusion. In addition, contractility parameters decreased with decreasing EHT size, indicating that difference are mainly due to the decrease in total cell number *pro rata* since any decrease in tissue thickness would actually enhance nutrient and oxygen availability by diffusion.

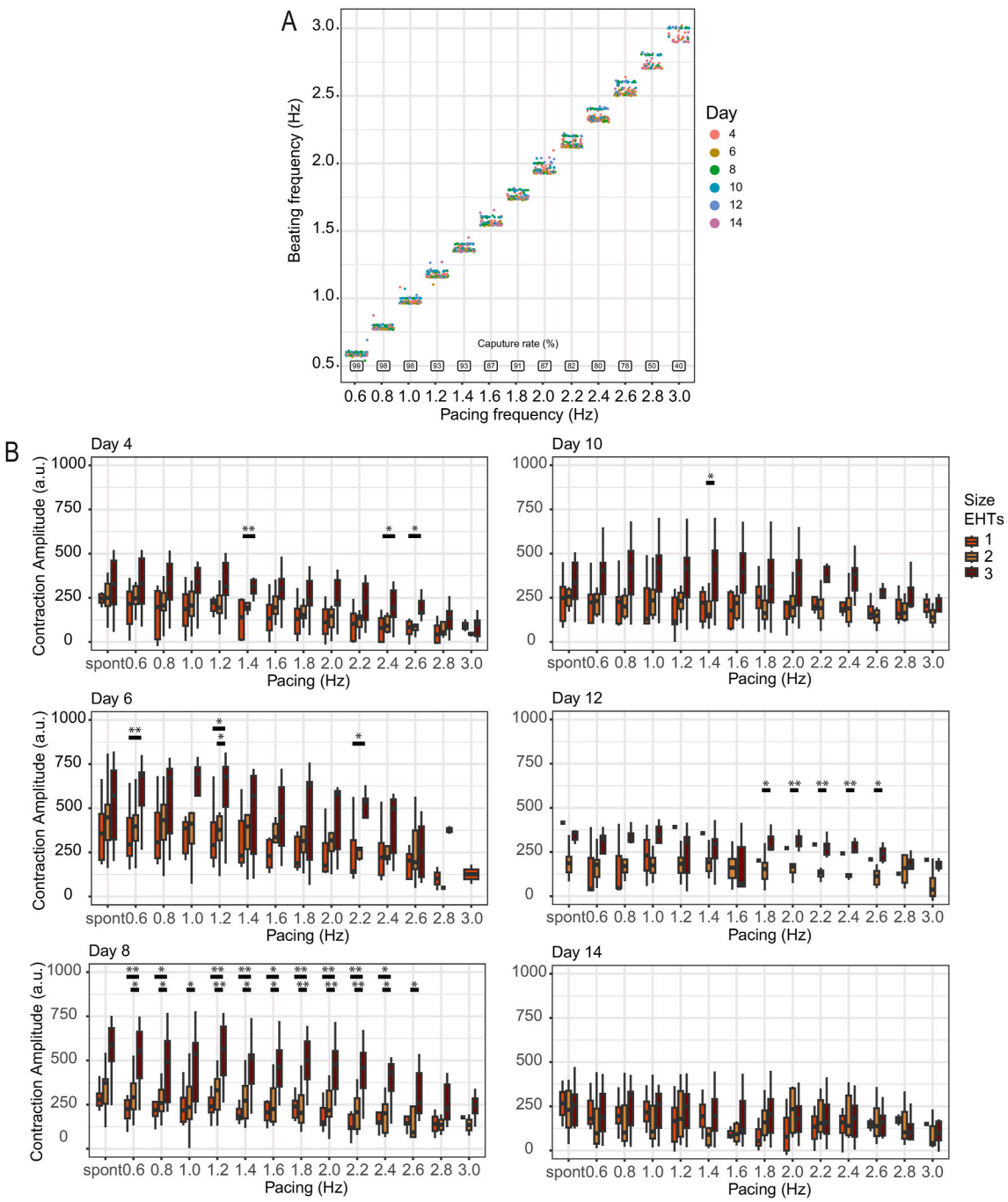

Fig. 4. EHTs follow electrical pacing between 0.6 and 3 Hz

(A) Beating frequency of EHTs size 1, 2 and 3 combined when paced between 0.6 and 3 Hz from day 4 to day 14. Overall capture rate is shown in percentage above the x-axis. **(B)** Contraction amplitude of spontaneous contracting EHTs and when electrically paced between 0.6 and 3 Hz of EHT size 1, 2 and 3 on day 4, 6, 8, 10, 12 and 14. N = 4; *p < 0.05; **p < 0.01; ***p < 0.001. Data is shown as mean ± SEM. N indicates EHTs from 4 independent batches per group. One-way Anova with Tukey *post hoc* test is shown.

To compare the functionality of the three downscaled EHT platforms with microwell volumes of 3, 2 and 1 μL, a total of 4.7×10^4, 3.1×10^4 and 1.6×10^4 cells per EHT, respectively. All cells were derived isogenically from the same hiPSC-derived cardiac mesoderm, paving the way for replacing one or more of the cardiac cell types with mutant variants for disease modelling. As mentioned earlier, Chen and colleagues generated a miniaturized EHT platform based entirely on neonatal CMs. Here, however, hiPSC-CMs combined with cardiac stromal cells were used for similar reasons but with the additional opportunities in the future for cardiac disease modelling as they can capture disease phenotypes and defective cellular signaling [14,15,27]. Even though less mature than neonatal heart cells, hiPSC-CMs offer advantages of unlimited supply and human genetic background [28].

Cells were thawed from frozen stock and mixed with ECM consisting of Collagen 1 and Matrigel, as described previously for standard EHTs [7]. This mimics to some extent connective tissue in the heart. The cells self-aggregated around the two elastomeric micropillars and were able to create a well-defined and beating network of cardiomyocytes in all three miniaturized EHTs, as in previous studies using larger EHTs [5,7,12]. Anchoring of the EHTs on the micropillars mimics the afterload in

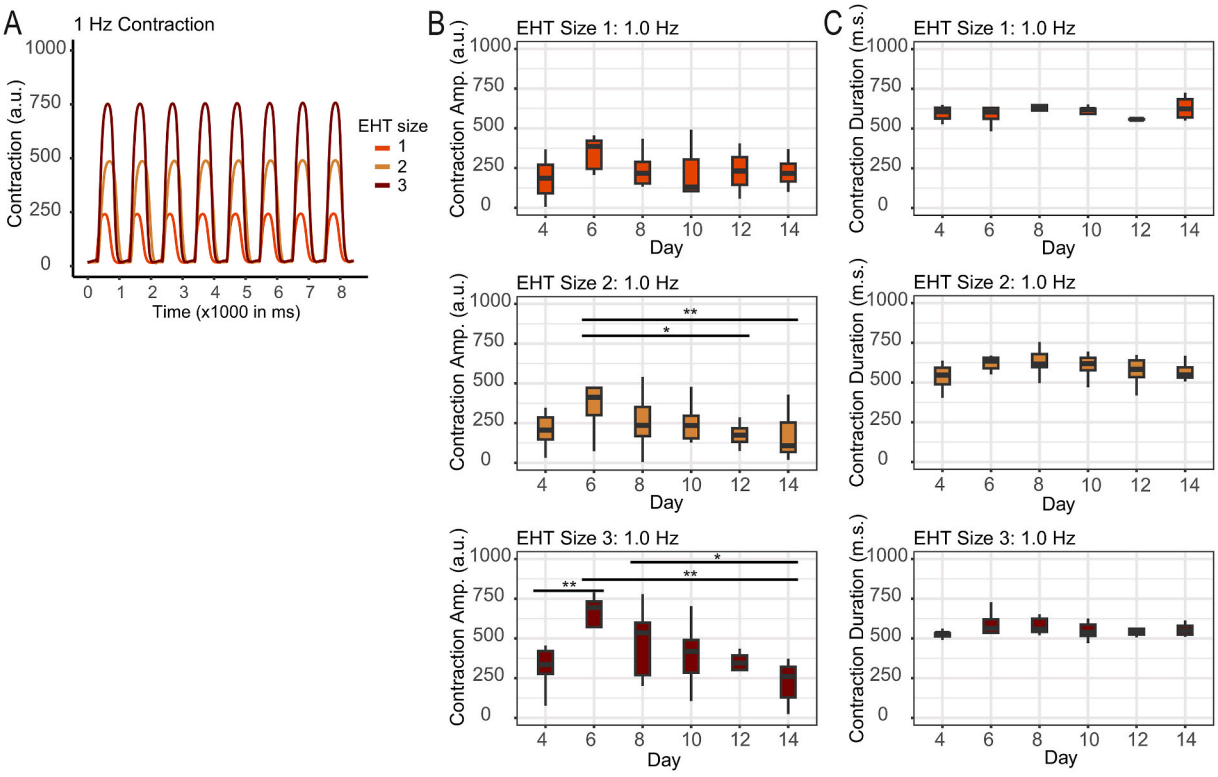

Fig. 5. Contraction amplitude over time and over frequency in size 1, 2 and 3 EHTS.
(A) Representative qualitative analysis of contraction of EHTs size 1, 2 and 3 that were electrically paced with 1 Hz on day 6. **(B)** Contraction amplitude of EHTs size 1, 2 and 3 between day 4 and 14 and electrically paced with 1 Hz. **(C)** Contraction duration of EHTs size 1, 2 and 3 between day 4 and 14 and electrically paced with 1 Hz. N = 4; *p < 0.05; **p < 0.01; ***p < 0.001. Data is shown as mean ± SEM. N indicates EHTs from 4 independent batches per group. One-way Anova with Tukey *post hoc* test is shown.

the native heart and promotes unidirectional contraction, which typically started within 72 h. Biomechanical load is known to enhance tissue maturation and construction of physiologically relevant models [29,30]. Consistent with our previous findings, we observed homogeneous cell distribution throughout the EHTs [16].

The viability of cells in the downscaled EHTs was demonstrated by staining for live and dead cells within the tissues. During imaging, contraction was stopped using para-nitroblebbistatin, a non-phototoxic and photostable myosin inhibitor, as an alternative to blebbistatin [31]. The relative cell viability was assessed on day 4 and 14 and showed a significant increase in the EHTs over time. This contrasts with an earlier study which showed declining cell viability after 7 days of EHT culture [15]. Additionally, the absolute cell number of live cells increased, while the number of dead cells remained unchanged, indicating cell proliferation within the tissues (Figs. S2C and D). This might be the proliferation of hiPSC-FBs, since we would not expect proliferation of hiPSC-CMs in light of our previous study on tri-cell type cardiac microtissues [20]. In addition, no necrotic clusters were observed in the EHTs; it is likely that nutrients and oxygen supplied by the medium can adequately reach all parts of the tissue.

Spontaneous beating of EHTs was detected from day 4 to day 14. The decline in contraction amplitude observed after day 10 was not attributable to cell death, as the cell viability remained constant. Furthermore, the results showed the appearance of more quiescent EHTs over time indicating decreased functionality. Therefore day 14 might be the maximum time that the miniaturized EHTs can actually be used in assays. Nevertheless, these results are comparable with other studies, where only 30% of the tissues contracted spontaneously or contraction rate decreased over time, in some cases to quiescence by day 10 [32,33]. In addition, the contraction duration of the spontaneous tissue we observed was between 500 and 1500 ms, which is comparable to other EHT studies [10,11]. Notably, the EHTs remained responsive to external electrical stimulation, although contraction amplitude did decrease. Reduced functionality was first evident after 10 days so this might represent the true time limit for any assays using the model.

We successfully electrically stimulated EHTs of all sizes within a physiologically relevant range. Electrical pacing was performed during the measurements on day 4, 6, 8, 10, 12 and 14, one well at a time and for less than 1 min at each frequency. The methodology was limited by the need to manually reposition the electrodes for each technical repeat. Incorporating electrodes into the EHT platform would facilitate automation and enable more reproducible and long-term stimulation of the tissues. We demonstrated that electrical pacing between 0.6 and 2 Hz was followed by more than 85% of the EHTs. The capture rate decreased rapidly to below 50% for pacing stimulation higher than 2.6 Hz. The maximum capture rate between 2 and 3 Hz was similar in all three downscaled EHTs and as shown by others although, some studies reported higher capture rates when continuous electrical pacing was used to “train” the EHTs [4,10,34,35]. The highest mean contraction amplitude was reached on day 6 when pacing at a physiologically relevant frequency of 1 Hz. However, fluctuations in contractility were observed within the first few days of pacing. This might be due to the pillar design: the pillars are straight and therefore the EHTs tend to “crawl” upwards to the top of the pillars. In some experiments, the EHTs even “jumped off” the pillars completely. This difference in z-direction position results in differences in mechanical load that affects the force generated. Overall, the optimal timeframe for conducting assays based on contraction amplitude was indicated as being between day 6 and 8 for EHTs of size 2 and 3, as they exhibited the widest range of contraction.

EHTs are particularly suited to measuring changes in contraction force, as the deflection and stiffness of the micropillars can be used to calculate the applied force. While moderate afterload is known to

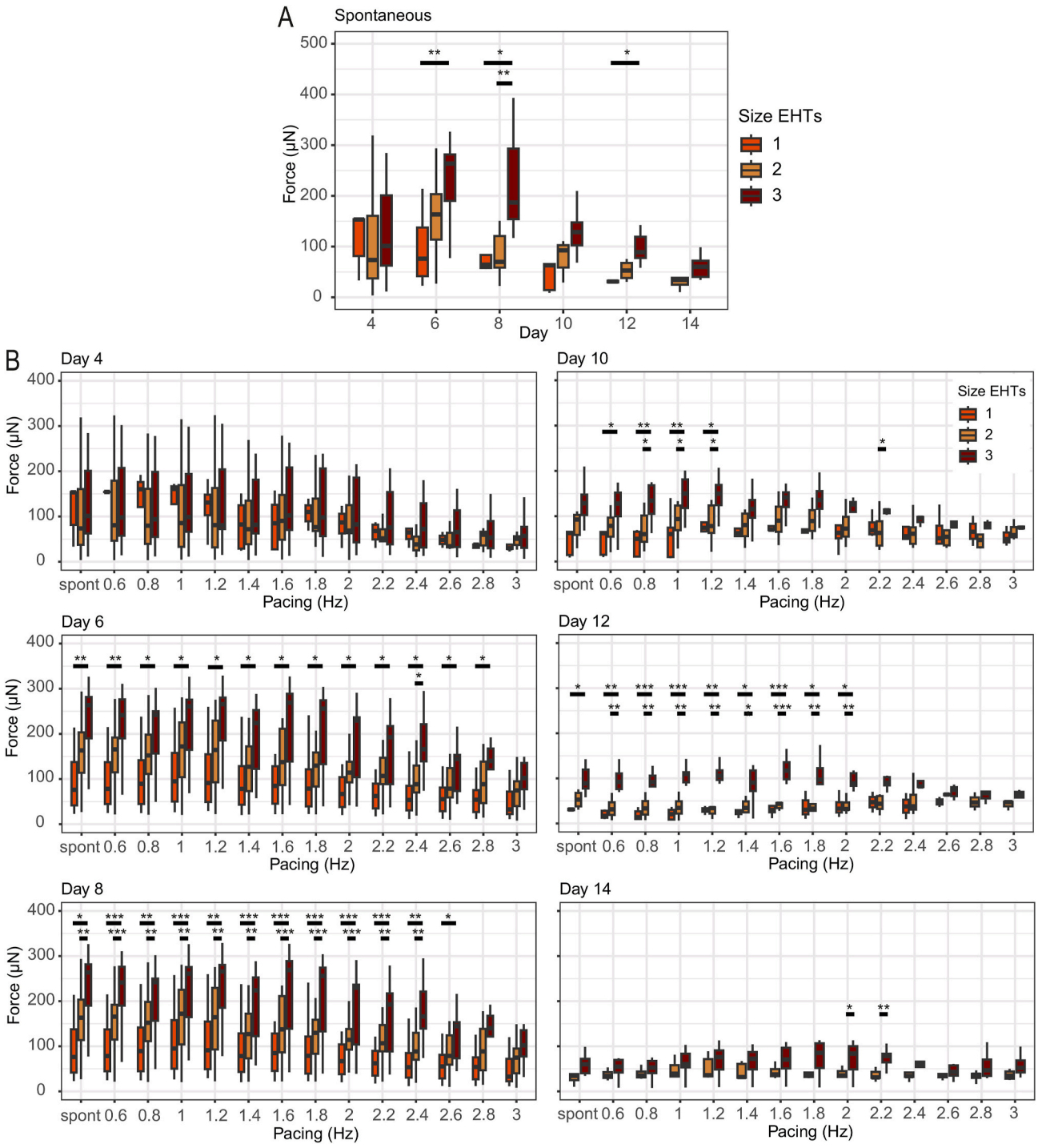

Fig. 6. Contractile force and normalized contractile force per cell in downscaled EHTs.
(A) Spontaneous contraction force of EHTs size 1, 2 and 3 between day 4 and 14. **(B)** Contraction force of spontaneous contracting and electrically paced EHTs between 0.6 and 3 Hz of EHTs size 1, 2 and 3 on day 4, 6, 8, 10, 12 and 14. **(C)** Contraction force normalized for total cell number per EHT of spontaneous contracting EHTs and when electrically paced between 0.6 and 3 Hz of EHTs size 1, 2 and 3 on day 4, 6, 8, 10, 12 and 14. N = 4; *p < 0.05; **p < 0.01; ***p < 0.001. Data is shown as mean ± SEM. N indicates EHTs from 4 independent batches per group. One-way Anova with Tukey *post hoc* test is shown.

promote cardiomyocyte maturation, excessive increases may be detrimental and lead to pathological changes [36]. The most significant disparities in contractile force (recorded for spontaneous beating and electric pacing, respectively) were observed on day 8, with force demonstrating a positive correlation with tissue size. This followed expectations, since the number of contractile cells is higher in the larger EHTs. After day 8, contractile force gradually decreased in all EHTs and fell below the detection limit for size 1 EHTs by day 14. Others reported that maximum active force of EHTs is typically between 150 and 500 µN, which is comparable to force measured in our EHTs even though we used significantly fewer cells per EHT [4,5,7,13,37].We recommend day 8 as the optimal time for conducting assays related to contraction force in our platform. Furthermore, on day 8, assessments can be made for both spontaneous contraction and electrical pacing frequencies ranging

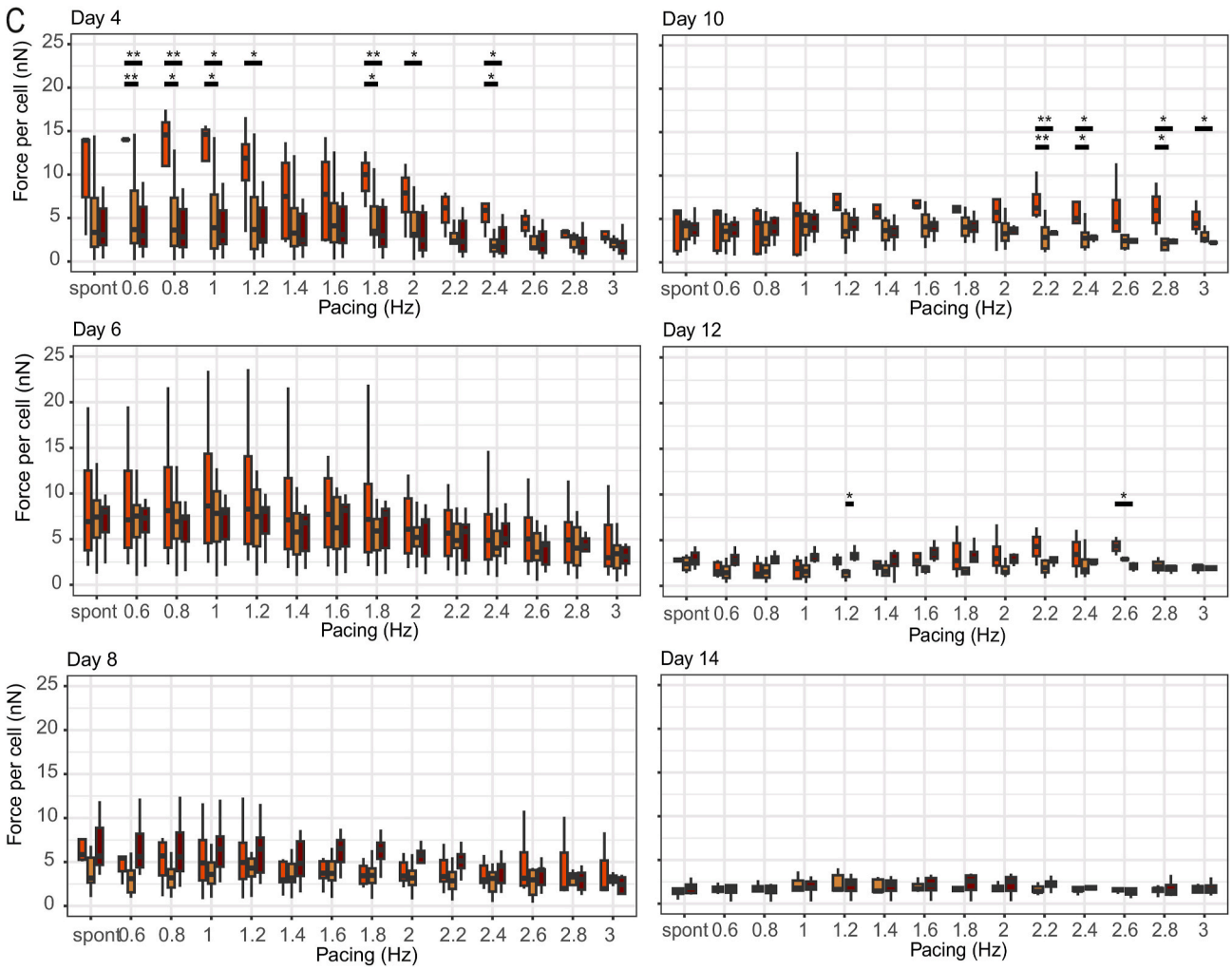

Fig. 6. (*continued*).

from 0.6 to 2.4 Hz. One limitation of this short optimal time window is that our model would then be most suitable only for acute drug responses. For example, inotropic or toxic drugs, that often have an acute response.

Upon normalization for cell number, we observed a higher contractile force in size 1 EHTs compared to size 2 and 3 at specific pacing frequencies on day 4. In line with previous reports, the difference in contractile force is likely attributable to a higher load per cell in size 1 EHTs compared to larger EHTs with more cells [36,38]. Although differences in contraction kinetics were observed between the different sizes of EHTs on day 6 and day 8, the normalized force of contraction remained similar on these days, confirming day 8 as the optimal time for conducting assays.

The reliability of these data is impacted by the possible variation in position of EHTs on the micropillars. Ideally, the position should be defined and identical across all samples. Here, we measured the starting position of the EHT on the z-axis of the micropillars was in the middle but during contraction the EHTs tended to move up the micropillars and eventually "jump" off, which resulted in variability over time and loss of datapoints. Success rates in different experiments were between 0% (i.e. all EHTs moved off the pillars) and 90% (i.e. very few were lost) and the highest average success rate was found for size 2 EHTs. In ongoing research, we are developing an EHT platform which allows precise positioning of EHTs on the z-axis by "waisting" at the mid-point [39].

The spontaneous beating of the EHTs here was comparable to our previous 3D microtissue model also based on 3 cell-types [20]. In these microtissues, the relatively low beat rate was paralleled by increased cardiomyocyte maturation markers. Since we did not measure the maturation markers as such in our EHTs, we cannot attribute reduced spontaneous beating to increased maturation. However, since we were able to stimulate the EHTs to more physiologically relevant beating frequencies, we demonstrate fully functional tissues. We do note, however, that some studies using only hiPSC-CM to form EHTs show more physiologically relevant spontaneous beating rates [4,5,13].

In sum, previous studies reported EHTs typically requiring 0.5–2 million cells [3,7,10,11]. Our study is distinct in using just 16,000 cells in the smallest format and all cells are derived from hiPSC. A limitation of size 1 EHTs is that manual seeding of the platform is more difficult compared to the larger EHTs, and can result in damage of the microwell or pillars. For manual seeding, our preference is for size 2 or 3 EHTs. In addition, the latter exhibited a larger range of contractile parameters compared to size 1 EHTs. For example, a higher contraction amplitude range might be required to detect minor changes in inotropy in response to drugs or disease. Robotics could in the future make production for the preferred size at scale feasible. In addition, future experiments are needed to test contraction kinetics after day 14 to validate downscaled EHTs for the use of chronic drug testing. As is, our downscaled EHT model provides a physiologically relevant and cost-effective alternative to conventional EHTs.

8. Author contributions

LW, CM, BM contributed to conception and design of the study. LW performed the lab work and drafted the manuscript. MW analysed the data and performed the statistical analysis. LW and MW made the figures. MD, MM, PS contributed to conception and design of the EHT platforms. MD manufactured the EHT platforms, and provided technical input. PS and CM secured funding. PS, MM, MB, CM and BM provided supervision of the work. All authors contributed to manuscript revision, read, and approved the submitted version.

9. Funding

This work was supported by the Netherlands Organ-on-Chip Initiative, an NWO Gravitation project (024.003.001) funded by the Ministry of Education, Culture and Science of the government of the Netherlands, European Research Council (ERC-CoG 101001746) Mini-HEART, and Novo Nordisk Foundation Center for Stem Cell Medicine supported by Novo Nordisk Foundation grants (NNF21CC0073729).

Declaration of competing Interest

CM is co-founder of Pluriomics (now Ncardia) and BM is co-founder and CTO of Demcon Biovitronix. The other authors declare that the research was conducted in the absence of any commercial or financial relationships that could be construed as a potential conflict of interest.

Acknowledgments

We thank J. Hudson and the Cardiac Bioengineering Research Group at QIMR Berghofer for helping setting up the EHT protocol. Dr Valeria Orlova is thanked for guidance in hiPSC-EC differentiation. Dorien Ward-van Oostwaard, Viviana Meraviglia, Ruben van Helden, Giulia Campostrini are thanked for guidance in hiPSC-CM, hiPSC-EC and hiPSC-CF differentiation. We thank the people from LUMC microscope facility for their support during imaging.

Appendix A. Supplementary data

Supplementary data to this article can be found online at https://doi.org/10.1016/j.bbrc.2023.09.034.

References

[1] J.U.G. Wagner, S. Dimmeler, Cellular cross-talks in the diseased and aging heart, J. Mol. Cell. Cardiol. 138 (Jan. 2020) 136–146, https://doi.org/10.1016/J.YJMCC.2019.11.152.
[2] G. Campostrini, et al., Generation, functional analysis and applications of isogenic three-dimensional self-aggregating cardiac microtissues from human pluripotent stem cells, Nat. Protoc. 16 (4) (Apr. 2021) 2213, https://doi.org/10.1038/S41596-021-00497-2.
[3] N.L. Tulloch, et al., Growth of engineered human myocardium with mechanical loading and vascular coculture, Circ. Res. 109 (1) (Jun. 2011) 47–59, https://doi.org/10.1161/CIRCRESAHA.110.237206.
[4] I. Mannhardt, et al., Human engineered heart tissue: analysis of contractile force, Stem Cell Rep. 7 (1) (2016) 29–42, https://doi.org/10.1016/j.stemcr.2016.04.011.
[5] M.N. Hirt, et al., Functional improvement and maturation of rat and human engineered heart tissue by chronic electrical stimulation, J. Mol. Cell. Cardiol. 74 (Sep. 2014) 151–161, https://doi.org/10.1016/J.YJMCC.2014.05.009.
[6] L. Sala, et al., Musclemotion: a versatile open software tool to quantify cardiomyocyte and cardiac muscle contraction in vitro and in vivo, Circ. Res. 122 (3) (Feb. 2018) e5–e16, https://doi.org/10.1161/CIRCRESAHA.117.312067/-/DC1.
[7] R.J. Mills, et al., Functional screening in human cardiac organoids reveals a metabolic mechanism for cardiomyocyte cell cycle arrest, Proc. Natl. Acad. Sci. U. S. A. 114 (40) (2017) E8372–E8381, https://doi.org/10.1073/pnas.1707316114.
[8] U. Saleem, et al., Blinded, multicenter evaluation of drug-induced changes in contractility using human-induced pluripotent stem cell-derived cardiomyocytes, Toxicol. Sci. 176 (1) (Jul. 2020) 103–123, https://doi.org/10.1093/toxsci/kfaa058.
[9] A. Eder, I. Vollert, A. Hansen, T. Eschenhagen, Human engineered heart tissue as a model system for drug testing, Adv. Drug Deliv. Rev. 96 (Jan. 2016) 214–224, https://doi.org/10.1016/J.ADDR.2015.05.010.
[10] K. Ronaldson-Bouchard, et al., Advanced maturation of human cardiac tissue grown from pluripotent stem cells, Nature 556 (7700) (2018) 239–243, https://doi.org/10.1038/s41586-018-0016-3.
[11] S. Schaaf, et al., Human engineered heart tissue as a versatile tool in basic research and preclinical toxicology, PLoS One 6 (10) (2011), 26397, https://doi.org/10.1371/journal.pone.0026397.
[12] J.L. Ruan, et al., Mechanical stress conditioning and electrical stimulation promote contractility and force maturation of induced pluripotent stem cell-derived human cardiac tissue, Circulation 134 (20) (2016) 1557–1567, https://doi.org/10.1161/CIRCULATIONAHA.114.014998.
[13] M.D. Lemoine, et al., Human iPSC-derived cardiomyocytes cultured in 3D engineered heart tissue show physiological upstroke velocity and sodium current density, Sci. Rep. 7 (1) (2017), https://doi.org/10.1038/s41598-017-05600-w.
[14] W.R. Legant, A. Pathak, M.T. Yang, V.S. Deshpande, R.M. McMeeking, C.S. Chen, Microfabricated tissue gauges to measure and manipulate forces from 3D microtissues, Proc. Natl. Acad. Sci. USA 106 (25) (Jun. 2009) 10097–10102, https://doi.org/10.1073/pnas.0900174106.
[15] T. Boudou, et al., A microfabricated platform to measure and manipulate the mechanics of engineered cardiac microtissues, Tissue Eng. 18 (9–10) (May 2012) 910–919, https://doi.org/10.1089/ten.tea.2011.0341.
[16] M. Dostanić, et al., A miniaturized EHT platform for accurate measurements of tissue contractile properties, J. Microelectromech. Syst. 29 (5) (Oct. 2020) 881–887, https://doi.org/10.1109/JMEMS.2020.3011196.
[17] LUMCi028-A. https://hpscreg.eu/cell-line/LUMCi028-A, 2021.
[18] C.W. Van Den Berg, D.A. Elliott, S.R. Braam, C.L. Mummery, R.P. Davis, Differentiation of human pluripotent stem cells to cardiomyocytes under defined conditions, Methods Mol. Biol. 1353 (2014) 163–180, https://doi.org/10.1007/7651_2014_178/FIGURES/4.
[19] V.V. Orlova, F.E. Van Den Hil, S. Petrus-Reurer, Y. Drabsch, P. Ten Dijke, C. L. Mummery, Generation, expansion and functional analysis of endothelial cells and pericytes derived from human pluripotent stem cells, Nat. Protoc. 9 (6) (2014) 1514–1531, https://doi.org/10.1038/nprot.2014.102.
[20] E. Giacomelli, et al., Human-iPSC-Derived cardiac stromal cells enhance maturation in 3D cardiac microtissues and reveal non-cardiomyocyte contributions to heart disease, Cell Stem Cell 26 (6) (2020), https://doi.org/10.1016/j.stem.2020.05.004.
[21] C.B. Sim, et al., Sex-specific control of human heart maturation by the progesterone receptor, Circulation 143 (16) (Apr. 2021) 1614–1628, https://doi.org/10.1161/CIRCULATIONAHA.120.051921/FORMAT/EPUB.
[22] R.L. Carrier, M. Rupnick, R. Langer, F.J. Schoen, L.E. Freed, G. Vunjak-Novakovic, Perfusion improves tissue architecture of engineered cardiac muscle, Tissue Eng. 8 (2) (Apr. 2002) 175–188, https://doi.org/10.1089/107632702753724950.
[23] M. Radisic, J. Malda, E. Epping, W. Geng, R. Langer, G. Vunjak-Novakovic, Oxygen gradients correlate with cell density and cell viability in engineered cardiac tissue, Biotechnol. Bioeng. 93 (2) (Feb. 2006) 332–343, https://doi.org/10.1002/bit.20722.
[24] H.K. Voges, S.R. Foster, L. Reynolds, R.J. Mills, E.R. Porrello, J.E. Hudson Correspondence, Vascular cells improve functionality of human cardiac organoids, Cell Rep. (2023), 112322, https://doi.org/10.1016/j.celrep.2023.112322.
[25] I. Vollert, et al., In-vitro perfusion of engineered heart tissue through endothelialized channels, Tissue Eng. 20 (2013), 131025032956001, https://doi.org/10.1089/ten.TEA.2013.0214.
[26] U. Arslan, et al., Vascularized hiPSC-derived 3D cardiac microtissue on chip, Stem Cell Rep. 18 (7) (Jul. 2023) 1394–1404, https://doi.org/10.1016/j.stemcr.2023.06.001.
[27] Y. Shiba, et al., Allogeneic transplantation of iPS cell-derived cardiomyocytes regenerates primate hearts, Nature 538 (7625) (2016) 388–391, https://doi.org/10.1038/nature19815.
[28] K. Bourque, J. Jones-Tabah, D. Pétrin, R.D. Martin, J.C. Tanny, T.E. Hébert, Comparing the signaling and transcriptome profiling landscapes of human iPSC-derived and primary rat neonatal cardiomyocytes, Sci. Rep. 13 (1) (Jul. 2023), 12248, https://doi.org/10.1038/s41598-023-39525-4.
[29] M.N. Hirt, et al., Increased afterload induces pathological cardiac hypertrophy: a new in vitro model, Basic Res. Cardiol. 107 (6) (Nov. 2012) 307, https://doi.org/10.1007/s00395-012-0307-z.
[30] R. Truitt, et al., Increased afterload augments sunitinib-induced cardiotoxicity in an engineered cardiac microtissue model, JACC Basic Transl Sci 3 (2) (Apr. 2018) 265–276, https://doi.org/10.1016/j.jacbts.2017.12.007.
[31] M. Køpiró, et al., Enzyme inhibition para-nitroblebbistatin, the non-cytotoxic and photostable myosin II inhibitor, Angew. Chem. Int. 53 (2014) 8211–8215, https://doi.org/10.1002/anie.201403540.
[32] C.P. Jackman, A.L. Carlson, N. Bursac, Dynamic culture yields engineered myocardium with near-adult functional output, Biomaterials 111 (Dec. 2016) 66–79, https://doi.org/10.1016/j.biomaterials.2016.09.024.
[33] Y. Zhao, et al., A platform for generation of chamber specific cardiac tissues and disease modelling HHS Public Access, Cell 176 (4) (2019) 913–927, https://doi.org/10.1016/j.cell.2018.11.042.
[34] M. Szepes, et al., Dual function of iPSC-derived pericyte-like cells in vascularization and fibrosis-related cardiac tissue remodeling in vitro, Int. J. Mol. Sci. 21 (23) (Nov. 2020) 8947, https://doi.org/10.3390/ijms21238947.
[35] M. Tiburcy, et al., Defined engineered human myocardium with advanced maturation for applications in heart failure modeling and repair, Circulation 135

(19) (May 2017) 1832–1847, https://doi.org/10.1161/CIRCULATIONAHA.116.024145.
[36] A. Leonard, et al., Afterload promotes maturation of human induced pluripotent stem cell derived cardiomyocytes in engineered heart tissues, J. Mol. Cell. Cardiol. 118 (1) (May 2018) 147–158, https://doi.org/10.1016/j.yjmcc.2018.03.016.
[37] G. Kensah, et al., Murine and human pluripotent stem cell-derived cardiac bodies form contractile myocardial tissue in vitro, Eur. Heart J. 34 (15) (Apr. 2013) 1134–1146, https://doi.org/10.1093/eurheartj/ehs349.
[38] N. Hersch, et al., The constant beat: cardiomyocytes adapt their forces by equal contraction upon environmental stiffening, Biol Open 2 (3) (Mar. 2013) 351–361, https://doi.org/10.1242/bio.20133830.
[39] M. Dostanić, et al., Highly reproducible tissue positioning with tapered pillar design in engineered heart tissue platforms, in: 2023 IEEE 36th International Conference on Micro Electro Mechanical Systems (MEMS), IEEE, Jan. 2023, pp. 374–377, https://doi.org/10.1109/MEMS49605.2023.10052166.